

Cite this: *Chem. Sci.*, 2026, 17, 1676

All publication charges for this article have been paid for by the Royal Society of Chemistry

# Fabricating liquid crystal actuators: from small pre-strain to large actuation strain

Enjian He,<sup>a</sup> Yixuan Wang,<sup>a</sup> Yanjin Yao,<sup>a</sup> Yang Yang,<sup>b</sup> Zhijun Yang,<sup>a</sup> Hongtu Xu,<sup>a</sup> Huan Liang,<sup>b</sup> Jiujiang Ji,<sup>a</sup> Guoli Wang,<sup>c</sup> Yen Wei<sup>a</sup> and Yan Ji<sup>\*a</sup>

Liquid crystal elastomers (LCEs) are emerging as compelling materials for soft actuators, sensors, and artificial muscles, due to their reversible and anisotropic deformation upon external stimuli. Incorporating dynamic covalent bonds into LCE networks (xLCEs) introduces reconfigurability and enables programmable actuation through stimuli-activated reversible bond exchange reactions. However, traditional programming approaches typically require large pre-strains at elevated temperatures to induce sufficient mesogen orientation and network rearrangement for large actuation strains, which imposes significant processing constraints. Here, we report an efficient method to fabricate monodomain xLCE actuators with large actuation strains using small pre-strains (as low as 10%). By tuning thermal programming parameters such as temperature and time, we demonstrate that high and tunable actuation can be achieved through the cooperative orientation of mesogens and network rearrangement *via* bond exchange. Comparative studies with non-liquid crystalline dynamic polymer networks and LCEs without dynamic covalent bond exchange allow us to further understand how large actuation strain can be accessed under minimal mechanical deformation. Moreover, spatial programming of actuation strain is realized by local control over bond exchange kinetics, enabling complex and heterogeneous deformation modes within a monolithic xLCE film.

Received 15th October 2025

Accepted 31st October 2025

DOI: 10.1039/d5sc07967e

rsc.li/chemical-science

## 1. Introduction

Liquid crystal elastomers (LCEs) are a class of polymers with bidirectional shape-memory effects in response to external stimuli such as heat, light, or electric and magnetic fields, making them highly promising for soft robotics, smart textiles, and other applications.<sup>1–3</sup> Their actuation behavior fundamentally relies on the orientation of mesogens and the reversible transition between liquid crystal (LC) and isotropic phases. In polydomain LCEs, where LC domains are randomly oriented, only local ordering occurs upon phase change, resulting in negligible macroscopic actuation. By contrast, aligning the mesogens into a monodomain state *via* methods such as mechanical stretching, surface anchoring, or shear extrusion, enables pronounced and reversible macroscopic actuation.<sup>3,4</sup> Recently, dynamic LCEs (xLCEs) incorporating exchangeable bonds have offered new method to monodomain fabrication and structure reprogramming.<sup>5</sup> These dynamic bonds allow stress-induced mesogen orientation to be fixed *via* stimuli-

activated bond exchange reactions, while also enabling network topology rearrangement, repair, welding, and reprocessing.<sup>6,7</sup>

Despite the prospects of xLCEs, challenges remain in their processing and performance control. The conventional monodomain LCE method, involving sequential mechanical orientation and photo or thermal crosslinking processes, necessitates elongation close to the fracture strain to achieve mesogen orientation.<sup>8–10</sup> Even when programming xLCEs *via* post-orientation after polymerization, large pre-strain is still typically needed to achieve sufficient orientation.<sup>11</sup> Most thermally activated dynamic networks require heating above the isotropic transition temperature ( $T_i$ ) to initiate bond exchange, where the material softens and becomes mechanically fragile, making it more susceptible to failure under large strains.<sup>12</sup> Beyond these processing limitations, the actuation strain in existing xLCE systems is largely determined by chemical formulation (for example: type and content of mesogen,<sup>13–15</sup> crosslinking density,<sup>16–18</sup> reaction between monomers<sup>19,20</sup> *etc.*), demanding careful and complex molecular design to tailor actuation strain. This reliance on “composition-defined performance” poses barriers to achieving spatially heterogeneous or gradient actuation within a single film.

In this study, we report the unexpected but reasonable finding that applying remarkably small pre-strains (as low as 10%) during programming enables xLCEs to achieve large actuation strains far exceeding the initial deformation, yielding

<sup>a</sup>The Key Laboratory of Bioorganic Phosphorus Chemistry & Chemical Biology (Ministry of Education), Department of Chemistry, Tsinghua University, Beijing 100084, China

<sup>b</sup>Institute of Nuclear and New Energy Technology, Tsinghua University, Beijing 100084, China

<sup>c</sup>Electric Power Research Institute, China Southern Power Grid Co. Ltd, Guangzhou 510623, China. E-mail: jiyuan@mail.tsinghua.edu.cn



highly oriented monodomain LC actuators. This approach effectively circumvents material fracture and programming failures, challenging the conventional paradigm that large pre-strains are prerequisites for significant actuation. As the programming parameters (temperature, time, and pre-strain) affect both the extent of network rearrangement and the resulting actuation strains, spatially patterned programming of differential actuation strains is achievable within a single xLCE film. This strategy provides a straightforward yet effective route for manufacturing large scale, complex-shaped LC actuators with tunable and programmable performance.

To uncover the underlying mechanism, we systematically investigated the conditions under which this phenomenon arises and compared different crosslinking systems. These include non-liquid crystalline dynamic polymer networks (DPNs) and LCEs without dynamic covalent bond exchange. The preparation of monodomain xLCEs involves stretching the material to induce mesogen orientation, followed by dynamic covalent bond exchange that permanently fixes this orientation through network topology rearrangement. Experiments show that it takes sufficiently long time for the exchange reaction to fully fix the orientation state. This is the premise of obtaining large actuation strain through small pre-strain. Otherwise, small pre-strain can only obtain small actuation strain because the exchange reaction is not sufficient and the orientation state can only be partially fixed. This is also why small pre-strains can only produce small actuation strains in previous reports. In LCEs without dynamic covalent bonds, the orientation states generated by pre-strain are fixed through secondary crosslinking. While small pre-strains can produce actuation strains exceeding their magnitude, significant large actuation strains still require substantial pre-strain. This differs from xLCEs, presumably due to their pre-crosslinked network architecture and excessive fixation of polymer chain topology by the secondary crosslinking during programming, which restricts the effective reorientation of mesogens, thereby diminishing the achievable actuation strain. In comparison, xLCEs utilize dynamic network rearrangement to preferentially fix mesogen alignment, avoiding excessive polymer chain rearrangement and enabling large actuation strain even under small pre-strain.

## 2. Results and discussion

### 2.1. Preparation and basic characterization of xLCEs

To provide a model system for investigation, a self-catalyzed xLCE (S-xLCE) was selected (Fig. 1a). The liquid crystal oligomer (LCO) was synthesized *via* an efficient aza-Michael addition reaction between *n*-butylamine (*n*-BA) and the LC mesogen 1,4-bis-[4-(3-acryloyloxypropyloxy)benzoyloxy]-2-methylbenzene (RM257). By adjusting the molar feed ratio of acrylates to amines, the molecular weight of the resulting LCO could be controlled. Specifically, a higher acrylate excess led to lower molecular weights. For optimal actuation and mechanical performance, a molar ratio of 7 : 6 (acrylates to amines) was employed. Subsequently, photopolymerization of the acrylic double bonds was initiated using the photo initiator 2,2-dimethoxy-2-phenylacetophenone (DMPA), yielding the crosslinked S-xLCE network.

This system was chosen due to the presence of residual *n*-butylamine in the final network, which acts as an *in situ* tertiary amine catalyst. Previous studies have demonstrated that tertiary amines can catalyze transesterification reaction (Fig. 1b), enabling efficient network topology rearrangement without the need for externally added catalysts while ensuring uniform catalyst content throughout all samples.<sup>12</sup>

The reaction process was monitored by Fourier Transform Infrared Spectroscopy (FTIR, Fig. 1c and d). The characteristic IR signals of amines ( $\text{-NH}_2$  asymmetric and symmetric stretching at  $3366\text{ cm}^{-1}$  and  $3291\text{ cm}^{-1}$ ) disappeared after oligomerization, while the signal of acrylates ( $\text{=C-H}$  bending at  $810\text{ cm}^{-1}$ ) was significantly reduced. The resulting LCO exhibited an average molecular weight of approximately  $4700\text{ g mol}^{-1}$ , as determined by proton nuclear magnetic resonance ( $^1\text{H NMR}$ , Fig. S1). Following photopolymerization, the complete disappearance of the acrylate signals confirmed a high conversion of monomers. Swelling experiments further demonstrated the formation of the structural integrity of the network with a high gel fraction of 93.5% (Fig. S2).

Differential scanning calorimetry (DSC, Fig. 1e) revealed a glass transition temperature ( $T_g$ ) of  $9.4\text{ }^\circ\text{C}$  and a  $T_i$  of  $87.9\text{ }^\circ\text{C}$ , respectively. The S-xLCE showed excellent stability with a 1% weight loss temperature of  $215\text{ }^\circ\text{C}$  (Fig. S3). Rheological studies were performed to evaluate the dynamic properties of the material (Fig. 1f). Stress relaxation curves were measured at temperatures ranging from  $120\text{ }^\circ\text{C}$  to  $160\text{ }^\circ\text{C}$ , with the characteristic relaxation time ( $\tau^*$ ) defined as the time required for the stress to decay to  $1/e$  of its initial value. Increasing temperature accelerated the relaxation rate and decreased  $\tau^*$ , with the Arrhenius analysis of  $\ln \tau^*$  versus  $1/T$  confirming a temperature-dependent exchange behavior typical of vitrimer-like systems (Fig. 1g).<sup>21</sup> The activation energy ( $E_a$ ) for the transesterification reaction was calculated to be  $99.9\text{ kJ mol}^{-1}$ . The topology freezing transition temperature of the S-xLCE ( $T_v$ ) was determined *via* dilatometry to be  $162\text{ }^\circ\text{C}$  (Fig. 1h). The combined rheological and dilatometry results provided compelling evidence of the self-catalyzed transesterification behavior in the S-xLCE, supporting its role in enabling subsequent thermal programming and the formation of monodomain LC actuators.

### 2.2. Preparation of monodomain xLCEs with large actuation strains from small pre-strain

In polydomain LCE, the disordered orientation of mesogens hinders reversible actuation. This limitation can be overcome by programming xLCEs into a monodomain state.<sup>5</sup> In our programming procedure (Fig. 2a), the sample was subjected to a pre-strain, fixed at both ends with tape, and heated on a hot stage to facilitate dynamic bond exchange, thereby permanently locking the mesogen orientation. Following this programming step and subsequent cooling, the sample spontaneously elongated. Upon tape removal, it exhibited reversible actuation between heating and cooling. Conventional two-stage method typically requires large pre-strains (50–200%) to achieve sufficient mesogen orientation. Interestingly, we found that applying significantly smaller pre-strains, combined with





Fig. 1 Synthesis and characterization of the S-xLCE. (a) Synthesis and composition of the S-xLCE. (b) An illustration of the catalyst-free transesterification of the S-xLCE. (c and d) FTIR spectroscopy of the monomers, LCO and crosslinked S-xLCE film. (e) DSC curve of the S-xLCE. (f) Normalized shear stress relaxation curves of the S-xLCE at different temperatures. (g) Arrhenius plot depicting the measured characteristic relaxation time of the S-xLCE. (h) Dilatometry test of the S-xLCE.

controlled heating, was sufficient to fabricate monodomain xLCE actuators with large actuation strains. For the S-xLCE, programming at 150 °C for 80 min with a 20% pre-strain yielded a high actuation strain of 84%. Under the same conditions, a significantly smaller pre-strain of only 10% still achieved a nearly identical actuation strain of 80% (Fig. 2b).

To further validate the generality of our approach, we synthesized a biphenyl xLCE (BP-xLCE, Fig. S4 and S5) with ester free mesogens, which corresponds to the earliest reported xLCE system.<sup>11</sup> BP-xLCE films were programmed under 10% or 20% pre-strains at 180 °C for varying durations. As expected, a pre-strain as low as 10% yielded a high actuation strain of 73% (Fig. S6 and S7), while a 20% pre-strain resulted in a larger actuation strain of 79% (Fig. S8 and S9). These findings confirm that large actuation strains can be reliably achieved in xLCEs even under minimal pre-strain.

The experiment of BP-xLCE also excludes the possibility of an ester exchange reaction in the mesogen being the reason for large actuation strains achieved from small pre-strain in the S-xLCE. Prior studies have demonstrated that both aromatic and

aliphatic ester bonds are susceptible to exchange mediated by strong base catalysts at elevated temperatures, potentially leading to degradation of mesogenic structures, reduced T<sub>i</sub>, and compromised actuation performance.<sup>22</sup> However, heterolytic transesterification of these ester bonds typically requires higher activation energy than homolytic exchange. Given that the catalyst employed in the S-xLCE is an intramolecular tertiary amine and that the programming durations are relatively short, the occurrence of undesired exchange within the mesogenic units is presumed negligible under the current conditions.

### 2.3. The behavior of the S-xLCE under mechanical stretching without the involvement of transesterification: stretch induced macroscopic orientation

As the mechanical stretching is very important for the monodomain preparation, two different ways of mechanical stretching were investigated. The first one is the stress-strain response of the S-xLCE at room temperature, which is the same as the LCEs without dynamic covalent bonds, since bond exchange is





Fig. 2 (a) Schematic illustration and (b) photographs of achieving large actuation strain from small pre-strain after programming. Scale bars: 1 cm.

negligible under these conditions. At room temperature, the material remained in the nematic phase (Fig. S10). Upon mechanical loading, the S-xLCE initially exhibited elastic deformation, followed by a characteristic soft plateau region (Fig. 3a, *ca.* 30% to 100% strain).<sup>23</sup> In this region, the stress remained nearly constant despite increasing strain,

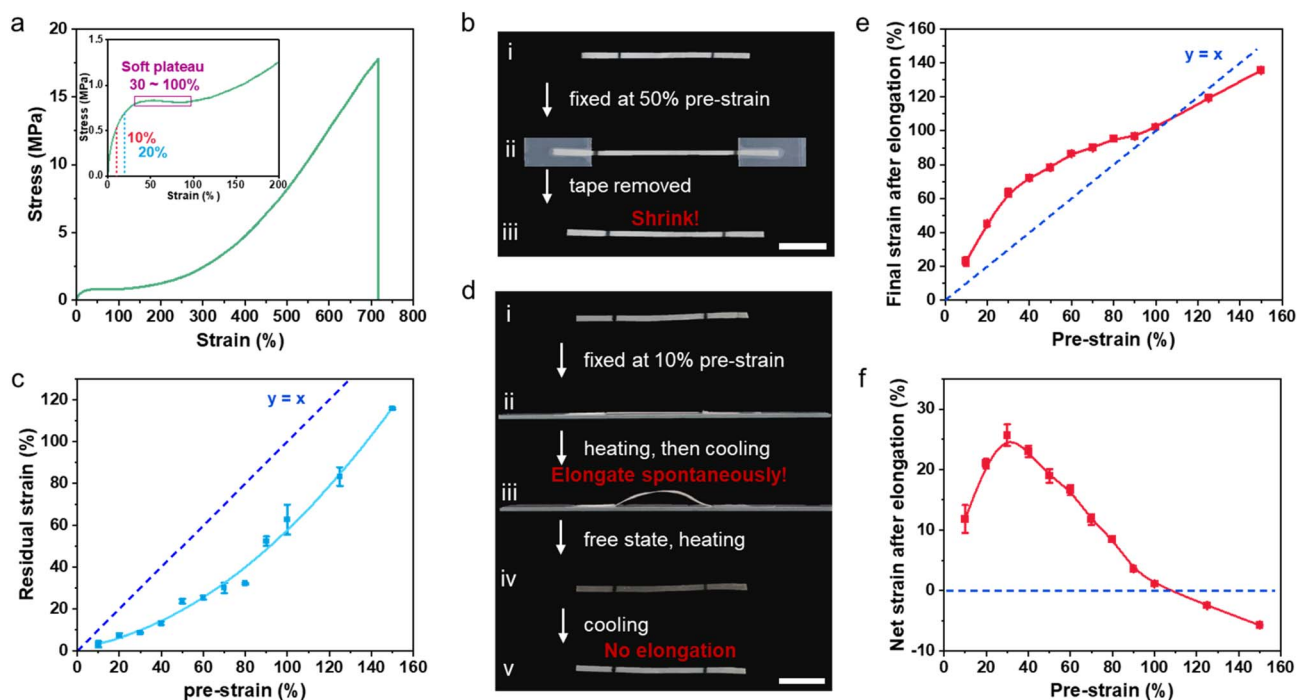


Fig. 3 (a) Stress-strain curve of the S-xLCE, with an inset showing a zoomed-in view of the 0–200% strain region. (b) Photographs of elastic recovery behavior of the S-xLCE after removal of tape. (c) Curves of residual strain of the polydomain S-xLCE after removal of tape. (d) Photographs of the spontaneous elongation behavior of spontaneous elongation of polydomain LCE without dynamic bond. (e) Curves of final strain after elongation versus pre-strain of the polydomain S-xLCE. (f) Curves of net elongation strain versus pre-strain of the polydomain S-xLCE. Scale bars: 1 cm.



corresponding to the gradual reorientation of LC domains along the loading direction.<sup>24</sup> Completion of this reorientation process marked the end of the plateau and resulted in increased nonlinearity in the stress–strain curve. Further deformation induced strain hardening as the network chains progressively oriented with the applied strain. After being stretched to a specific strain and unloaded, the material partially recovered its elastic deformation (Fig. 3b), with the residual strain in all cases being lower than the applied pre-strain (Fig. 3c).

The second one is similar to the monodomain preparation of the S-xLCE. S-xLCE films were subjected to 10% pre-strain using tape fixation and shortly heated at 110 °C (above  $T_i$ ), followed by cooling to room temperature. Owing to the relatively low temperature and short heating time, dynamic bond exchange is negligible. Upon cooling from the isotropic to the nematic state, the samples spontaneously elongated and buckled, and after tape removal their final length exceeded the initially applied pre-strain (Fig. 3d(i–iii)). The sample with 10% pre-strain spontaneously elongated to 123% of its original length after cooling. This elongation behavior is attributed to stress-induced orientation of mesogens along the loading direction, confirming the successful induction of temporary orientation, which is a phenomenon common to all LCE systems. Polarized optical microscopy (POM) confirmed the well-defined orientation within the S-xLCE before elongation (Fig. S11 and S12). Spontaneous elongation occurred across a pre-strain range of 10–100%, with larger pre-strains yielding larger final elongation (Fig. 3e). The net elongation strain, defined as the difference

between the elongated and pre-stretched lengths, reached a maximum of 26% at 30% pre-strain (Fig. 3f). However, when the pre-strain exceeded 100%, further increases suppressed elongation and even reversed to contraction upon tape removal, yielding a negative net strain. These observations are consistent with the soft plateau (30–100%) in the stress–strain curve of the S-xLCE (Fig. 3a).

S-xLCE under the above condition that suppress bond exchange is equivalent to a fully crosslinked, non-dynamic LCE. Therefore, once the constraint was removed, the sample no longer elongated and exhibited no actuation during subsequent heating–cooling cycles (Fig. 3d(vi and v)). In other words, LCEs cooled under small pre-strain applied in the isotropic phase can spontaneously elongate upon transitioning to the nematic phase. The key to achieving reversible actuation lies in the permanent fixation of the oriented state. In the S-xLCE, such fixation is achieved by topology rearrangement through dynamic bond exchange. In LCEs without dynamic covalent bonds, the fixation is done by the secondary crosslinking (like the two-stage method<sup>8</sup>).

#### 2.4. Fixation of pre-strain induced mesogen orientation

The permanent fixation of mesogen orientation induced by pre-strain is a prerequisite for actuation, and the degree of fixation directly determines the magnitude of actuation strain. Programming time is a key factor affecting the fixation. We observed a trend in xLCEs programmed under small pre-strains,



Fig. 4 (a) Photographs of the S-xLCE with 20% pre-strain after heating at 150 °C for 40 and 80 min. (b) The variation in actuation strain of the S-xLCE over programming time, with a heating temperature of 150 °C and the pre-strain controlled at 20%. (c) Actuation strain of the S-xLCE was obtained at different temperatures, with the pre-strain controlled at 20% and a heating time of 60 min. (d) The variation in actuation strain for the S-xLCE with different pre-strains, under various heating times at a controlled temperature of 150 °C. (e) The maximum actuation strain obtained by applying different pre-strains to the S-xLCE. (f) Time range required to obtain the maximum actuation strain by applying different pre-strains to the S-xLCE. Scale bars: 1 cm.



where the actuation strain initially increased with heating time to a maximum, followed by a gradual decline upon prolonged programming (Fig. 4a). This time-dependent behavior is clearly demonstrated in S-xLCE films programmed at 150 °C under 20% and 10% pre-strains. For the film under 20% pre-strain, the actuation strain peaked at 84% after 80 min before decreasing (Fig. 4b). A similar time-dependent trend was observed in samples with 10% pre-strain (Fig. S13). Actuation strain increased initially but decreased after prolonged heating. The maximum actuation reached 80%, slightly lower than that of the 20% pre-strained samples and required a longer heating time (100 min) to achieve.

The dependence of actuation strain on programming temperature further confirms that the magnitude of actuation is governed by the degree of orientation fixation.<sup>25</sup> To investigate this, S-xLCE films were pre-strained by 20% and heated for 60 min at temperatures ranging from 120 to 170 °C. As shown in Fig. 4c, actuation strain was limited at lower temperatures (120–130 °C), which we attribute to slow transesterification kinetics and insufficient network rearrangement, consistent with the stress relaxation behavior observed in Fig. 1f. As temperature increased, actuation strain rose significantly, reaching 61% at 140 °C and peaking at 82% at 150 °C. However, further increasing the temperature to 160–170 °C resulted in reduced actuation, likely due to excessive network rearrangement and stress relaxation. Given that 150 °C yielded optimal actuation strain with moderate relaxation kinetics, we selected this temperature for all subsequent S-xLCE programming experiments.

The dependence of actuation strain on pre-strain and time explains why the small pre-strain did not lead to large actuation strain in the past. Previous studies typically used short programming durations, which we identify as a limiting factor. We investigated the influence of varying pre-strains (30–100%) and heating times (10–30 min) on the resulting actuation strains. As shown in Fig. 4d, under short programming times (10 min), actuation strains increase with pre-strains, consistent with conventional reports.<sup>26,27</sup> In contrast, after longer programming (30 min), actuation strains across 30–100% pre-strain reach comparable values. For different pre-strains, the time necessary for the maximum actuation strain is different. Fig. 4e summarizes the maximum actuation strains under different pre-strains. Below 30% pre-strain, the maximum actuation gradually increases with pre-strain. Beyond this threshold, however, the strain plateaus at ~86%, indicating that once sufficient mesogen orientation and chain rearrangement are established, further pre-strain does not enhance the final actuation. Fig. 4f further shows that the time required to reach maximum actuation strain decreased significantly with increasing pre-strain: ~120 min for 10% pre-strain compared with ~10 min for 100% pre-strain. This can be understood by considering the accessibility of reactive sites of dynamic bond exchange. Since the transesterification rate is primarily governed by temperature and remains constant under isothermal programming conditions, the key variable becomes the spatial accessibility of dynamic exchange sites. At small pre-strains, bond exchange is restricted to local regions due to limited chain

extension, requiring longer times to fix sufficient mesogen orientation. On the contrary, larger pre-strains lead to greater chain extension, expanding the spatial accessibility of dynamic bonds and facilitating exchange over longer distances involves distant partners and reducing the time needed to reach peak actuation (Fig. S14). Although large pre-strains enable faster programming for the maximum actuation, they are not strictly necessary. With optimized heating times, similarly large actuation strains can also be realized at small pre-strains, providing greater versatility, and reducing mechanical demand. These results not only highlight the coupled yet distinct roles of pre-strain and programming time, but also explain why previous studies, which typically employed shorter programming durations, did not observe large actuation at small pre-strains.

## 2.5. Comparison with LCEs without dynamic covalent bonds

We carried out comparative experiments using acrylate-rich LCEs (A-LCEs), a conventional two-stage crosslinking system.<sup>8</sup> The A-LCE was synthesized *via* thiol–acrylate Michael addition, leaving excess acrylate groups for UV-triggered secondary crosslinking. This second-stage reaction locks mesogen orientation, enabling monodomain actuator production.<sup>28</sup> DSC confirmed a  $T_i$  of 75 °C (Fig. S15). The stress–strain curve of the polydomain A-LCE displayed a soft elastic plateau from 10% to 75% strain (Fig. S16), reflecting LC domain reorientation. When tested above  $T_i$  (90 °C), this plateau vanished and the film behaved as an isotropic rubber, exhibiting a lower elongation at break than at room temperature, which in turn restricted the maximum pre-strain applicable during programming (Fig. S17). To compare its fundamental response with the S-xLCE, we subjected the polydomain A-LCE to the same experimental conditions: cooling from the isotropic to the nematic phase under a pre-strain. This likewise resulted in spontaneous elongation and film buckling, confirming that this initial orientation behavior is common to both LCE systems (Fig. S18).

The fixation of mesogen orientation can be done either at room temperature or at a temperature above  $T_i$  (Fig. 5a). For samples UV-cured in the nematic phase, actuation strains remained below the applied pre-strain (Fig. 5b). The actuation strain increased rapidly with pre-strain but exhibited a slower growth beyond 75%. For example, a 12.5% pre-strain led to an actuation strain of 10.7% (0.86-fold to pre-strain), a 75% pre-strain led to an actuation strain of 65% (0.89-fold to pre-strain), while a 200% pre-strain yielded only 86% actuation (0.43-fold to pre-strain). In contrast, when the A-LCE was UV-cured in the isotropic phase to simulate xLCE processing conditions, actuation strains can exceed the applied pre-strain at low pre-strains (Fig. 5c). For example, a 12.5% pre-strain yielded 30% actuation (2.4-fold to pre-strain), while a 25% pre-strain produced 40% actuation (1.6-fold to pre-strain). This behavior, absent in nematic-crosslinked samples, resembles that of xLCEs. However, despite exceeding the pre-strain, the absolute actuation strain remained relatively low. Even as the actuation strain gradually increased with pre-strain, it reached no more than 52% even at 100% pre-strain. This performance is consistent





Fig. 5 (a) Schematic illustration of the UV-curing process for A-LCE actuators. (b and c) Actuation strain of A-LCE orientation fixed through UV exposure (b) at R.T. and (c) above  $T_i$ . (d) Comparison of different LCE systems.

with previous reports that large actuation strains generally require large pre-strains. In sharp contrast, the S-xLCE exhibits a more pronounced effect, achieving an actuation strain of 80% (8-fold the pre-strain) under only 10% pre-strain (Fig. 5d).

## 2.6. Analysis of length changes in different systems

We observed different length change of the sample between the S-LCE and A-LCE, which may contribute to the reason why usually large pre-strain is necessary to get large actuation strain for the A-LCE. For both samples, the final lengths measured at high temperature and at room temperature after monodomain preparation had increased relative to the original length. We use  $L_{\text{heat}}$  to refer the length increment of the sample measured at temperatures above  $T_i$ , while  $L_{\text{cool}}$  refer to the length increment measured at room temperature.

For the S-xLCE, under 20% pre-strain, when heated at 150 °C for varying durations, with increasing heating time, the sample length in both the heated and cooled states increased. Specifically,  $L_{\text{heat}}$  increased steadily, reaching 13% after 120 min (Fig. 6a). In contrast,  $L_{\text{cool}}$  increased rapidly during the first 80 min, peaking at 97%. A slight reduction in  $L_{\text{cool}}$  was observed beyond this point. The increase in  $L_{\text{heat}}$  is attributed to progressive topology rearrangement because of the polymer chains instead of mesogen orientation, as confirmed by a non-LC PEG-DPN reference system (Fig. S19–S21). In PEG-DPN, external force and heating induce network topological rearrangement through dynamic covalent bond exchange, enabling permanent fixation of the imposed deformation and exhibiting plasticity (Fig. 7a). The extent of rearrangement governs the degree of shape fixation, with more complete rearrangement enabling the material to better retain the imposed deformation,

eventually approaching the applied pre-strain under prolonged programming.<sup>29,30</sup> After programming, no reversible actuation was observed in PEG-DPN. Instead, transesterification led to permanent shape fixation, with  $L_{\text{cool}}$  and  $L_{\text{heat}}$  remaining nearly identical. In contrast, xLCEs exhibit a substantial difference between  $L_{\text{cool}}$  and  $L_{\text{heat}}$ , which stems from the presence of mesogens.<sup>31</sup> The programming of xLCEs involves not only polymer chain rearrangement but also strain-induced mesogen orientation fixation. We therefore attribute the difference between  $L_{\text{cool}}$  and  $L_{\text{heat}}$  ( $L_{\text{cool}} - L_{\text{heat}}$ ) to the progressive orientation fixation of mesogens, which is essential for the resulting actuation strain (Fig. 7b).

Further analysis is shown in Fig. 6b. The  $L_{\text{cool}}$ /pre-strain (reflecting total deformation) initially increases with time, reaching a peak before declining. This time-dependent behavior can be understood as the outcome of two competing processes (polymer chain rearrangement and mesogen orientation fixation) during bond exchange. At the early stage of programming, dynamic bond exchange primarily acts to fix the stress-induced mesogen orientation. In this regime, network rearrangement helps “lock in” the oriented mesogens, resulting in a continuous increase in actuation strain (Fig. 4a). However, as heating continues, polymer chains gradually undergo more extensive rearrangement, resulting in a decrease in actuation strain after reaching its maximum. Correspondingly,  $L_{\text{heat}}$  gradually approached the initial pre-strain value of 20% under extended heating (Fig. 6a). As indicated by the blue curve in Fig. 6b, relative contribution from polymer chain rearrangement remained relatively low, generally below 10%.

For the A-LCE, the increase in  $L_{\text{heat}}$  is attributed to progressive fixation of aligned polymer chains by secondary





Fig. 6 (a, c and e) Length increment under heating and cooling conditions. (b, d and f) The ratio of cooling length increment to pre-strain and decomposition of total deformation. (a and b) S-xLCE with 20% pre-strain programmed at 150 °C for varying durations. (c and d) A-LCE with different pre-strains UV cured in the nematic state. (e and f) A-LCE with different pre-strains UV cured in the isotropic state.

crosslinking, while the difference in  $L_{\text{cool}} - L_{\text{heat}}$  is also attributed to mesogen orientation (Fig. 7c). For the A-LCE UV-cured in the nematic phase,  $L_{\text{heat}}$  increased gradually with pre-strain up to 75%, then accelerated (Fig. 6c), consistent with the growing dominance of chain stretching beyond the soft elasticity plateau (Fig. S16). Conversely, the  $L_{\text{cool}}$  increased sharply below 75% pre-strain and slowed thereafter, highlighting the saturation of domain reorientation. POM confirmed this transition, showing enhanced birefringence above 75% pre-strain (Fig. S22 and S23). In Fig. 6d, analysis revealed that above 75% pre-strain, the relative contribution from mesogen orientation decreases while polymer chain crosslinking becomes dominant ( $L_{\text{heat}}/L_{\text{cool}}$  increase from 10% to 20%). This saturation of domain

reorientation leads to the deceleration in actuation gain. These results confirm that in A-LCEs secondarily crosslinked in the nematic state, the inherent domain structure prevents actuation strain from exceeding the pre-strain, and achieving large actuation necessitates large pre-strains to engage polymer chain deformation.

For the A-LCE UV-cured in the isotropic phase, as shown in Fig. 6e, both  $L_{\text{cool}} - L_{\text{heat}}$  and  $L_{\text{heat}}$  increased nearly proportionally with pre-strain. Notably,  $L_{\text{cool}}$  consistently exceeded the applied pre-strains, indicating that UV crosslinking effectively fixed the stress-induced mesogen orientation (Fig. 6e and f). POM images revealed uniform birefringence and transmittance across pre-strain levels (Fig. S24 and S25), confirming well





Fig. 7 Schematic illustration and comparative analysis of the contributions to length increments: (a) PEG-DPN. (b) S-xLCE. (c) A-LCE (UV cured in the isotropic state).

orientation. As the blue line shown in Fig. 6f,  $L_{\text{heat}}/L_{\text{cool}}$  (reflecting polymer chain crosslinking) in isotropic-crosslinked samples reached nearly 40% at 100% pre-strain, substantially higher than the  $\sim 21\%$  observed in nematic-crosslinked systems even at 200% pre-strain. Although isotropic-crosslinked samples attained larger total deformation, their actuation strains were lower than their nematic-crosslinked counterparts at the same pre-strain. This limitation stems from excessive polymer chain topology fixation during isotropic UV curing, which restricts the reversible mesogen reorientation essential for large actuation strains.

Based on the above analysis, the difference in  $L_{\text{heat}}$  provides a clear explanation for why the S-xLCE can achieve high actuation strain under small pre-strains, whereas the A-LCE cannot. In the A-LCE,  $L_{\text{heat}}$  increases significantly with pre-strain (Fig. 6c and d). While the pre-crosslinked network is essential for maintaining mechanical integrity, the critical limitation for actuation performance comes from the subsequent UV crosslinking. This process permanently locks the polymer chains into a new conformation without allowing topological rearrangement, resulting in a pronounced rise in  $L_{\text{heat}}$ . In stark contrast, the S-xLCE exhibits only a minimal increase in  $L_{\text{heat}}$  across varying pre-strains (Fig. 5a and S26). xLCEs operate through a programming mechanism based on stress-induced mesogen orientation coupled with network rearrangement mediated by dynamic bond exchange. This synergy allows the network to adaptively rearrange and fix the oriented mesogen structure under small pre-strains.

## 2.7. Spatially programmable actuation in xLCEs

To overcome the limitations of “composition-defined performance” and enable spatially heterogeneous actuation within a single material, we demonstrate a strategy to spatially regulate actuation strain by locally tuning the degree of topology

rearrangement. By systematically modulating programming parameters such as pre-strain, programming temperature, and time, a broad range of actuation strains can be achieved (Fig. 8a).

As a proof of concept, we fabricated monolithic S-xLCE films in which distinct regions were programmed under different conditions to yield spatially heterogeneous actuation. In a representative example, a single S-xLCE film uniformly pre-strained at 10% and programming for different time, one half was heated at 150 °C for 60 min, while the other half underwent extended heating for 100 min (Fig. S27). This simple variation in heating time resulted in markedly different actuation responses: 44% actuation strain on the left and 82% on the right (Fig. 8b). This strategy stands in contrast to previously reported strategies that relied on irreversible degradation of mesogens to encode spatial actuation, which compromises repeatability and structural integrity. In contrast, our method enables reversible adjustment of actuation strain, solely through modulation of bond exchange kinetics without damaging the structure of mesogen.

Furthermore, by spatially varying the programming temperature, actuation gradients can also be achieved. In Fig. 8c, a square shape S-xLCE film was uniformly pre-strained by 20%, but individual edges were programmed at different temperatures: 140 °C for the top edge and 150 °C for the remaining sides. Upon actuation, the asymmetry in the strain response transformed the original square into a trapezoidal shape, with an actuation strain of 54% for the top edge and 80% for the other edges.

Finally, we explored the dependence of pre-strain on the magnitude of applied pre-strain under the same programming conditions. By selectively applying pre-strains 40, 60 and 80% to different edges within a single material and programming at 150 °C for 10 min, we generated a spatially heterogeneous





Fig. 8 (a) The actuation strain of xLCEs is tunable by adjusting the programming pre-strain, temperature, and time. (b–d) Spatially actuation strains were achieved by locally tuning the degree of topology rearrangement through modulation of (b) programming time, (c) programming temperature, and (d) applied pre-strain. Scale bars: 1 cm.

actuator exhibiting diverse actuation strains (Fig. 8d). This strategy of tailoring actuation strain through multi parameter modulation provides a robust toolkit for the design of sophisticated soft actuator, enabling programmable and spatially resolved deformation modes within a single material platform.

### 3. Conclusion

In this work, we report a previously overlooked programming method for xLCEs that enables large actuation strains to be achieved from remarkably small pre-strains. Contrary to the conventional requirement of large pre-strain, our experiments reveal that applying a small pre-strain by allowing extended time for dynamic bond exchange is sufficient to fix stress-induced mesogen orientation and produce a monodomain actuator. Critically, the method requires extended programming time, a factor that had been neglected in earlier xLCE programming studies. Unlike conventional LCEs, where secondary crosslinking leads to excessive polymer chain fixation and restricted actuation, xLCEs utilize dynamic network rearrangement to preferentially fix mesogen orientation with minimal chain rearrangement.

Furthermore, by leveraging this programming strategy, we demonstrate the spatial integration of heterogeneous actuation domains within a monolithic xLCE film through controlled variation in pre-strain, programming time, and temperature.

This versatile and composition independent approach offers a powerful strategy for constructing complex, large scale, reconfigurable xLCE actuators and significantly broadens the material design space for adaptive and multifunctional soft robots.

### Author contributions

E. He and Y. Ji proposed and designed the project. Y. Ji supervised the research. E. He performed all the experiments with the help of Y. Wang and Z. Yang. E. He and Y. Ji wrote the paper with the help of Y. Wang, Y. Yao, Y. Yang, H. Xu, H. Liang, and J. Ji provided valuable suggestions. G. Wang, Y. Wei, and Y. Ji provided funding support. All authors discussed the results and commented on the manuscript.

### Conflicts of interest

The authors declare no competing interests.

### Data availability

All the relevant data of this study are available within the manuscript and its supplementary information (SI). Supplementary information is available. See DOI: <https://doi.org/10.1039/d5sc07967e>.



## Acknowledgements

This work was supported by the Key Technologies Research and Development Program of China (2023YFB2407100) and National Natural Science Foundation of China (no. 22375114 (Y. Ji) and 21788102 (Y. Wei)).

## References

- 1 M. Chen, M. Gao, L. Bai, H. Zheng, H. J. Qi and K. Zhou, Recent Advances in 4D Printing of Liquid Crystal Elastomers, *Adv. Mater.*, 2023, **35**, 2209566.
- 2 E. M. Terentjev, Liquid Crystal Elastomers: 30 Years After, *Macromolecules*, 2025, **58**, 2792–2806.
- 3 Z.-C. Jiang, Q. Liu, Y.-Y. Xiao and Y. Zhao, Liquid crystal elastomers for actuation: A perspective on structure-property-function relation, *Prog. Polym. Sci.*, 2024, **153**, 101829.
- 4 K. M. Herbert, H. E. Fowler, J. M. McCracken, K. R. Schlafmann, J. A. Koch and T. J. White, Synthesis and alignment of liquid crystalline elastomers, *Nat. Rev. Mat.*, 2022, **7**, 23–38.
- 5 M. O. Saed, A. Gablier and E. M. Terentjev, Exchangeable Liquid Crystalline Elastomers and Their Applications, *Chem. Rev.*, 2022, **122**, 4927–4945.
- 6 Z. Wang and S. Cai, Recent progress in dynamic covalent chemistries for liquid crystal elastomers, *J. Mater. Chem. B*, 2020, **8**, 6610–6623.
- 7 C. Zhang, X. Lu, Z. Wang and H. Xia, Progress in Utilizing Dynamic Bonds to Fabricate Structurally Adaptive Self-Healing, Shape Memory, and Liquid Crystal Polymers, *Macromol. Rapid Commun.*, 2022, **43**, 2100768.
- 8 C. M. Yakacki, M. Saed, D. P. Nair, T. Gong, S. M. Reed and C. N. Bowman, Tailorable and programmable liquid-crystalline elastomers using a two-stage thiol-acrylate reaction, *RSC Adv.*, 2015, **5**, 18997–19001.
- 9 L. Liu, M.-H. Liu, L.-L. Deng, B.-P. Lin and H. Yang, Near-Infrared Chromophore Functionalized Soft Actuator with Ultrafast Photoresponsive Speed and Superior Mechanical Property, *J. Am. Chem. Soc.*, 2017, **139**, 11333–11336.
- 10 D. J. Roach, C. Yuan, X. Kuang, V. C.-F. Li, P. Blake, M. L. Romero, I. Hammel, K. Yu and H. J. Qi, Long Liquid Crystal Elastomer Fibers with Large Reversible Actuation Strains for Smart Textiles and Artificial Muscles, *ACS Appl. Mater. Interfaces*, 2019, **11**, 19514–19521.
- 11 Z. Pei, Y. Yang, Q. Chen, E. M. Terentjev, Y. Wei and Y. Ji, Mouldable liquid-crystalline elastomer actuators with exchangeable covalent bonds, *Nat. Mater.*, 2014, **13**, 36–41.
- 12 Q. Chen, W. Li, Y. Wei and Y. Ji, Reprogrammable 3D Liquid-Crystalline Actuators with Precisely Controllable Stepwise Actuation, *Adv. Intell. Syst.*, 2021, **3**, 2000249.
- 13 H. Guo, M. O. Saed and E. M. Terentjev, Thiol-acrylate side-chain liquid crystal elastomers, *Soft Matter*, 2022, **18**, 4803–4809.
- 14 M. Barnes, S. Cetinkaya, A. Ajnsztajn and R. Verduzco, Understanding the effect of liquid crystal content on the phase behavior and mechanical properties of liquid crystal elastomers, *Soft Matter*, 2022, **18**, 5074–5081.
- 15 B. R. Donovan, H. E. Fowler, V. M. Matavulj and T. J. White, Mechanotropic Elastomers, *Angew. Chem., Int. Ed.*, 2019, **58**, 13744–13748.
- 16 M. O. Saed, A. H. Torbati, C. A. Starr, R. Visvanathan, N. A. Clark and C. M. Yakacki, Thiol-acrylate main-chain liquid-crystalline elastomers with tunable thermomechanical properties and actuation strain, *J. Polym. Sci. Pt. B-Polym. Phys.*, 2017, **55**, 157–168.
- 17 M. O. Saed, R. H. Volpe, N. A. Traugott, R. Visvanathan, N. A. Clark and C. M. Yakacki, High strain actuation liquid crystal elastomers via modulation of mesophase structure, *Soft Matter*, 2017, **13**, 7537–7547.
- 18 B. Jin, Z. Zhu, T.-W. Wong and G. Chen, Network Topology Optimization for Alignment Programming of a Dynamic Liquid Crystalline Organo-Gel, *ACS Macro Lett.*, 2023, **12**, 1486–1490.
- 19 H. Liang, S. Zhang, Y. Liu, Y. Yang, Y. Zhang, Y. Wu, H. Xu, Y. Wei and Y. Ji, Merging the Interfaces of Different Shape-Shifting Polymers Using Hybrid Exchange Reactions, *Adv. Mater.*, 2023, **35**, e2202462.
- 20 H. Lu, M. Wang, X. Chen, B. Lin and H. Yang, Interpenetrating Liquid-Crystal Polyurethane/Polyacrylate Elastomer with Ultrastrong Mechanical Property, *J. Am. Chem. Soc.*, 2019, **141**, 14364–14369.
- 21 D. Montarnal, M. Capelot, F. Tournilhac and L. Leibler, Silica-Like Malleable Materials from Permanent Organic Networks, *Science*, 2011, **334**, 965.
- 22 G. Chen, H. Feng, X. Zhou, F. Gao, K. Zhou, Y. Huang, B. Jin, T. Xie and Q. Zhao, Programming actuation onset of a liquid crystalline elastomer via isomerization of network topology, *Nat. Commun.*, 2023, **14**, 6822.
- 23 M. Warner, P. Bladon and E. Terentjev, “Soft elasticity” — deformation without resistance in liquid crystal elastomers, *J. Phys. II*, 1994, **4**, 93–102.
- 24 T. J. White and D. J. Broer, Programmable and adaptive mechanics with liquid crystal polymer networks and elastomers, *Nat. Mater.*, 2015, **14**, 1087–1098.
- 25 R. G. Ricarte, S. Shanbhag, D. Ezzeddine, D. Barzycki and K. Fay, Time-Temperature Superposition of Polybutadiene Vitrimers, *Macromolecules*, 2023, **56**, 6806–6817.
- 26 X. Zhou, B. Jin, Z. Zhu, J. Wu, Q. Zhao and G. Chen, Metal-Ligand Bonds Based Reprogrammable and Re-Processable Supramolecular Liquid Crystal Elastomer Network, *Angew. Chem., Int. Ed.*, 2024, **63**, e202409182.
- 27 Y. Zhu, J. Huang, H. Mi, Z. Xu, Y. Ai, S. Gong, C. Li, M. Wang and L. Chen, Intrinsically Photothermal-Driven and Reconfigurable Liquid Crystal Elastomer Actuators Enabled by Multifunctional Dynamic Covalent Organic Photothermal Molecules, *Angew. Chem., Int. Ed.*, 2025, **64**, e202421915.
- 28 Y. Li, G. Parlato, F. K. Mase, R. M. Kasi, T. Zhang and X. Wang, Morphing of stiffness-heterogeneous liquid crystal elastomers via mechanical training and locally controlled photopolymerization, *Matter*, 2022, **5**, 4332–4346.



- 29 A. M. Hubbard, Y. Ren, A. Sarvestani, D. Konkolewicz, C. R. Picu, A. K. Roy, V. Varshney and D. Nepal, Recyclability of Vitriimer Materials: Impact of Catalyst and Processing Conditions, *ACS Omega*, 2022, 7, 29125–29134.
- 30 Z. Chen, X. Wang and Z. Li, Creep and recovery of vitrimers under thermo-chemo-mechanical coupling effects, *Polymer*, 2024, 311, 127567.
- 31 M. Chen, M. Gao, L. Bai, H. Zheng, H. J. Qi and K. Zhou, Recent Advances in 4D Printing of Liquid Crystal Elastomers, *Adv. Mater.*, 2022, 35, 2209566.

